AuthorA, P. C., D. M. AuthorB, and G. H. AuthorC, 2014: Template for properly formatted *Electronic Journal of Severe Storms Meteorology* submissions. *Electronic J. Severe Storms Meteor.*, **9** (2)**,** 1–6.

Electronic Journal of
SEVERE STORMS METEOROLOGY

Tornadic Mesocyclone Interactions and a Storm Tour Accident: The Lawrence-Linwood, Kansas High-precipitation Supercell of 28 May 2019

JONATHAN M. DAVIES
Kansas City, MO

(Submitted __ December 2019; in final form __ _____ 2020)

ABSTRACT

A tornado and mesocyclone occluded deep within a surging, rain-filled rear-flank downdraft (RFD) southwest of Lawrence, Kansas struck two vans of a storm tour company on 28 May 2019, causing several injuries. The location of this rain-wrapped tornado nearly two miles to the south of a larger developing mesocyclone was unexpected by both the tour group and several storm chasers nearby. Using radar data and storm chaser images, this paper documents the evolution of this tornado and its associated mesocyclone, as well as a subsequent interaction with a separate tornado and mesocyclone that preceded the formation of the large and long-track EF4 Lawrence-Linwood, Kansas tornado. In the wake of the storm tour accident, this event has ramifications for future spotter training regarding high-precipitation (HP) supercells.

1. Introduction

A large high-precipitation (HP) supercell (Doswell and Burgess 1993; Moller et al. 1994) developed at mid-afternoon on 28 May 2019 over east-central Kansas, going on to produce a large long-track EF4 tornado from southwest of Lawrence, Kansas (KS) to near Linwood, KS, ending just west of the Kansas City metropolitan area. The Lawrence-Linwood tornado was the first EF4 tornado to occur in northeast Kansas since 2003, yet no one was killed, due in part to excellent warnings and media coverage.

This HP supercell is noteworthy because a tornado prior to the Lawrence-Linwood tornado struck two vans of a storm tour company, resulting in several injuries. This tornado and associated mesocyclone were completely wrapped in rain within a surging rear-flank downdraft (RFD; Lemon and Doswell 1979), and located nearly two miles (3.2 km) to the south of a newly developing mesocyclone on radar that was also visible from storm chaser images. The original tornado and mesocyclone went on to combine with the new intensifying mesocyclone and a separate tornado, an interaction that occurred just before the formation of the large Lawrence-Linwood tornado.

The motivation for this paper is to document the storm evolution before, during, and just after the storm tour company incident, including the visually-hidden tornado that struck them, and the subsequent consolidation of mesocyclones and tornadoes precedent to the formation of the Lawrence-Linwood tornado. As a result, this paper will focus on storm evolution during the early tornadic phase of the HP supercell *southwest* of Lawrence prior to 2315 UTC. National Weather Service (NWS) radar data from Topeka, KS will be used, along with a ground survey of the event and photo/video images from storm chasers.

Because the evolution of this HP supercell was visually confusing to both the storm tour company and several storm chasers close by, ramifications for future spotter training will also be discussed.

Corresponding author address: Jon Davies, 4601 N. Main St., Kansas City, MO 64116, E-mail: davieswx@gmail.com

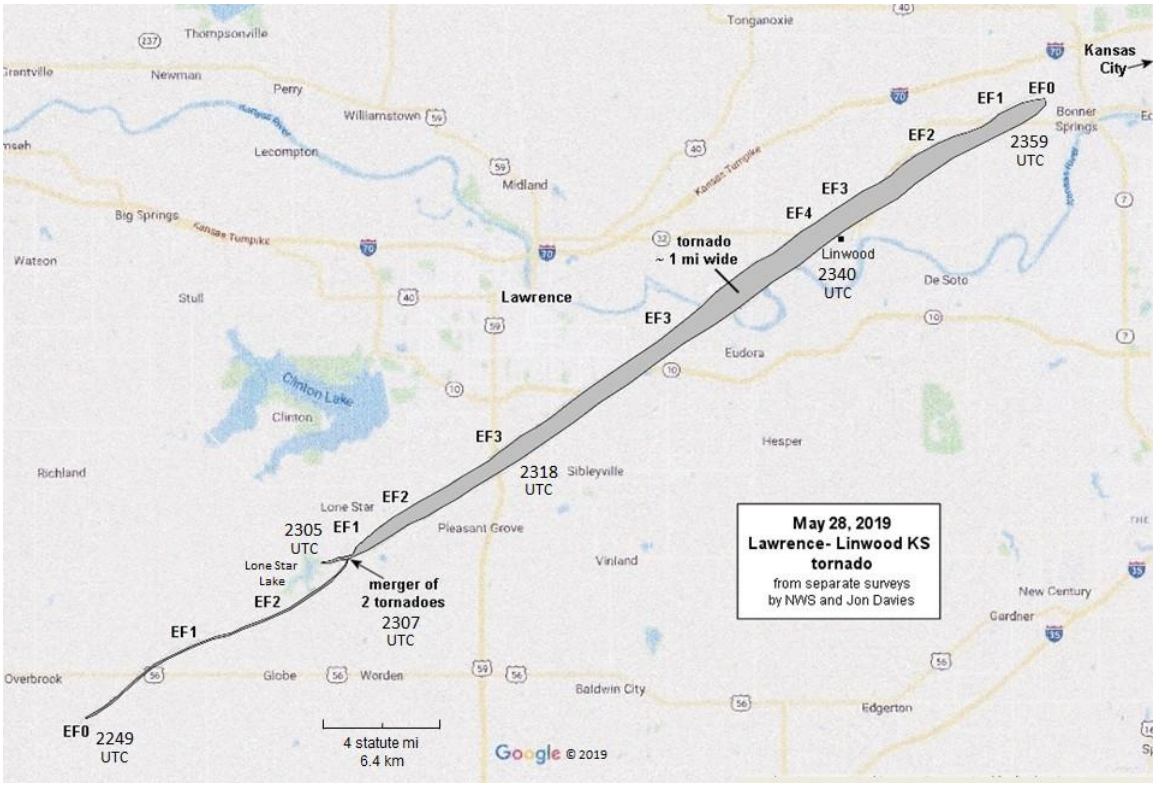

Figure 1. Damage tracks of the two main tornadoes associated with the 28 May 2019 Lawrence-Linwood, KS supercell, from combining separate ground surveys by NWS and the author.

2. The Lawrence-Linwood tornado

Figure 1 shows the paths and damage intensities at selected points of the two main tornadoes in northeast Kansas that occurred with the Lawrence-Linwood tornadic supercell, constructed from the author's own survey of the tracks and a separate survey by NWS. This includes the "merger"/consolidation of the two tornadoes southwest of Lawrence, which will be discussed in detail in sections 3, 4, and 5.

There isn't space here for a detailed analysis of meteorological conditions accompanying this event, but the environment over east-central and northeast Kansas on 28 May 2019 was quite supportive of tornadoes. Figure 2 shows that values of the effective-layer significant tornado parameter (Thompson et al. 2004) at 2100 UTC from the Storm Prediction Center (SPC) mesoanalysis were substantial over this area as storms formed within the warm sector south of a stationary front (see surface map in Fig. 3). Contrary to typical diurnal trends, the low-level jet (e.g., Palmén and Newton 1969; not shown) was increasing over eastern Kansas during the afternoon in response to a strong shortwave disturbance aloft in midlevels moving northeastward through the central

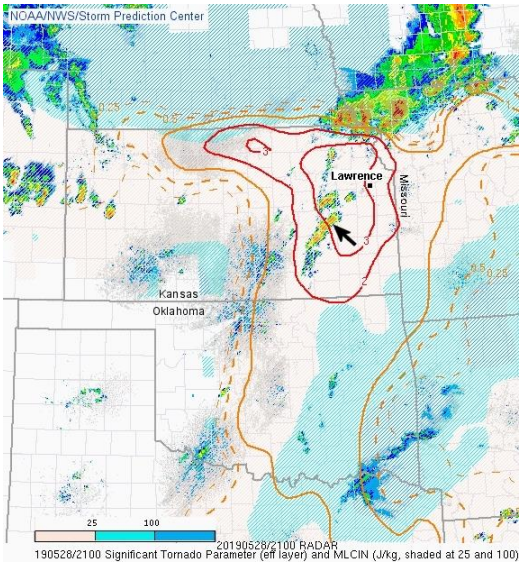

Figure 2. Significant tornado parameter (STP, effective-layer version, dimensionless) with MLCIN (J kg^{-1}) and composite radar base reflectivity from SPC mesoanalysis over Kansas, Missouri, and Oklahoma area at 2100 UTC on 28 May 2019. STP contours are gold and red; MLCIN >25 J kg^{-1} is shaded blue. Black arrow indicates storm cluster from which the Lawrence-Linwood supercell developed.

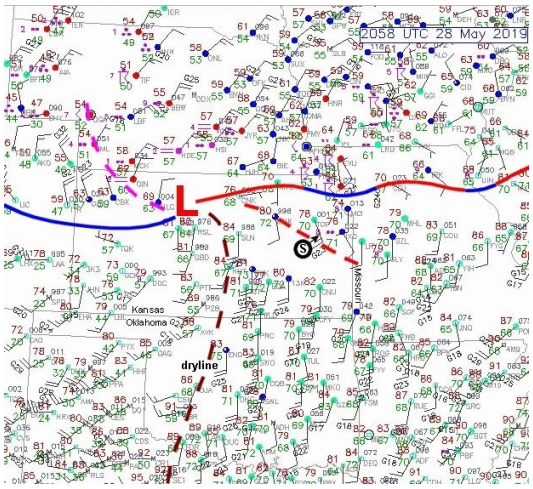

Figure 3. Surface observations (conventional) and frontal analysis over the central U.S. at 2100 UTC. The circled "S" shows the location of storm cluster noted in Fig. 2.

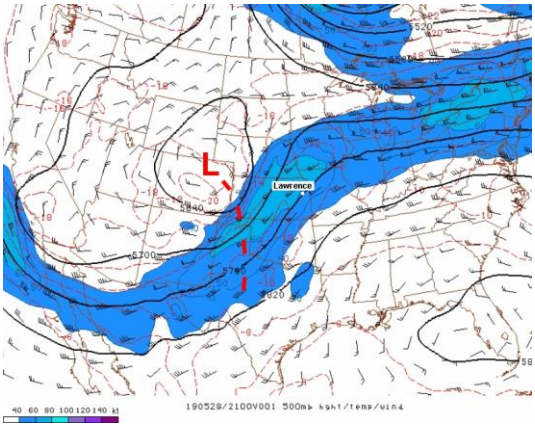

Figure 4. Objective analyses of 500 hPa winds (kt) and geopotential heights (m MSL) over the U.S. at 2100 UTC on 28 May 2019 from SPC mesoanalysis. Winds ≥40 kt are shaded blue, and temperature (°C) is analyzed in dashed red. Heavy red dashed line indicates shortwave associated with closed upper low (red "L").

Plains (see SPC 500 hPa analysis in Fig. 4). The resulting increase in low-level wind shear with strong instability already in place (e.g., Johns et al. 1993; not shown) contributed to the favorable environment for tornadic supercells suggested by Fig. 2.

The surface map analysis at 2100 UTC (Fig. 3) also suggests that a weak boundary, possibly a localized warm front (dashed heavy red line in Fig. 3), was oriented northwest to southeast over northeast Kansas, to the east and southeast of a surface low and to the south of the aforementioned stationary front. Winds were backed from a south-southeasterly direction just north of this boundary, which likely provided additional low-level wind shear to support tornadoes as a cluster of storms moving across the boundary coalesced into the tornadic HP supercell after 2200 UTC.

3. Radar evolution

Figure 5 is a 3-panel view of lowest elevation radar base reflectivity from the NWS Topeka radar showing the storm cluster over east-central Kansas evolving into the Lawrence-Linwood tornadic supercell as it crossed the weak boundary mentioned in the prior section. After a brief tornado with no damage at 2210 UTC south of Osage City, KS (shortly before Fig. 5b), the

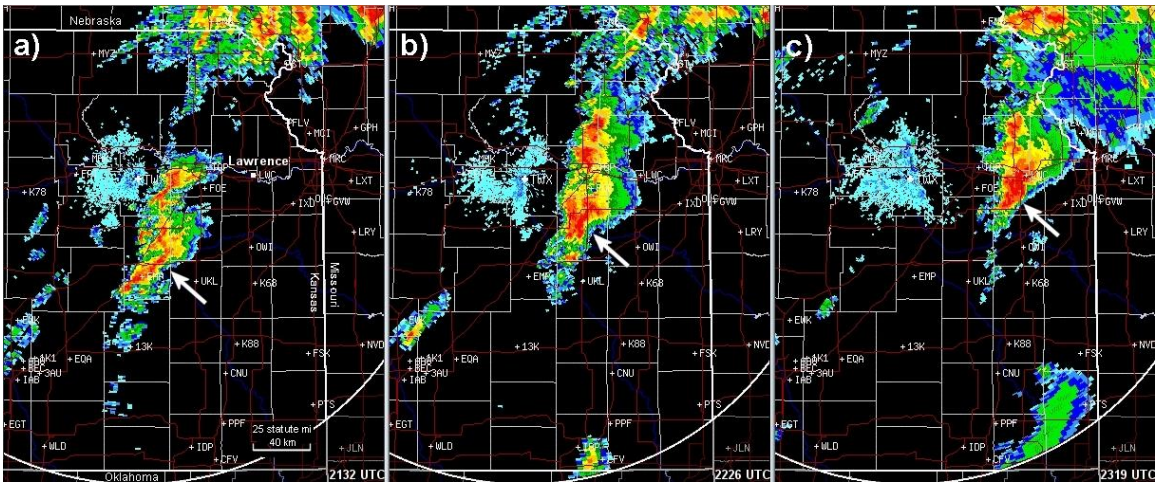

Figure 5. Base reflectivity (0.5 degree elevation) from Topeka NWS radar over eastern Kansas on 28 May 2019 at: a) 2132 UTC; b) 2226 UTC; and c) 2319 UTC. White arrow indicates storm cluster in a) that became Lawrence-Linwood HP supercell in b) and c). Large tornado was in progress in c).

first significant tornado began southeast of Overbrook, KS at 2249 UTC (between the times of Fig. 5b and 5c) and moved east-northeast roughly 10 miles (6 km) before combining with another newly-formed tornado northeast of Lone Star Lake around 2307 UTC (see Fig. 1).

The large Lawrence-Linwood tornado emerged from this interaction, and was in progress at the time of Fig. 5c. Notice from Fig. 5 that, as the storm cluster consolidated into a large but relatively discrete supercell, there were no storms to its south to interfere with environmental inflow characterized by strong low-level shear and instability supportive of tornadoes, discussed in the prior section.

Zooming in on the area southwest of Lawrence for greater detail, Fig. 6 shows lowest elevation storm-relative velocity from the Topeka radar (level 2 data) at roughly 6 minute intervals from 2253 UTC to 2311 UTC. In Fig. 6a, the original mesocyclone producing the tornado that touched down at 2249 UTC was indicated as a velocity couplet about to cross Highway 56 east of Overbrook, with a corridor of strong velocities flowing into it from the north. Six minutes later in Fig. 6b, the strongest velocities were farther north and east, with a new broad velocity couplet signaling the development of a large new mesocyclone north of the original mesocyclone (and tornado) that continued as a small velocity couplet 1.7 mi (2.7 km) south of the developing mesocyclone. Notice in Fig. 6b that a corridor of strong velocities from the northeast was now flowing into the developing northern mesocyclone, *not* the smaller original mesocyclone to its south.

About seven minutes later in Fig. 6c, both mesocyclones were still indicated as separate

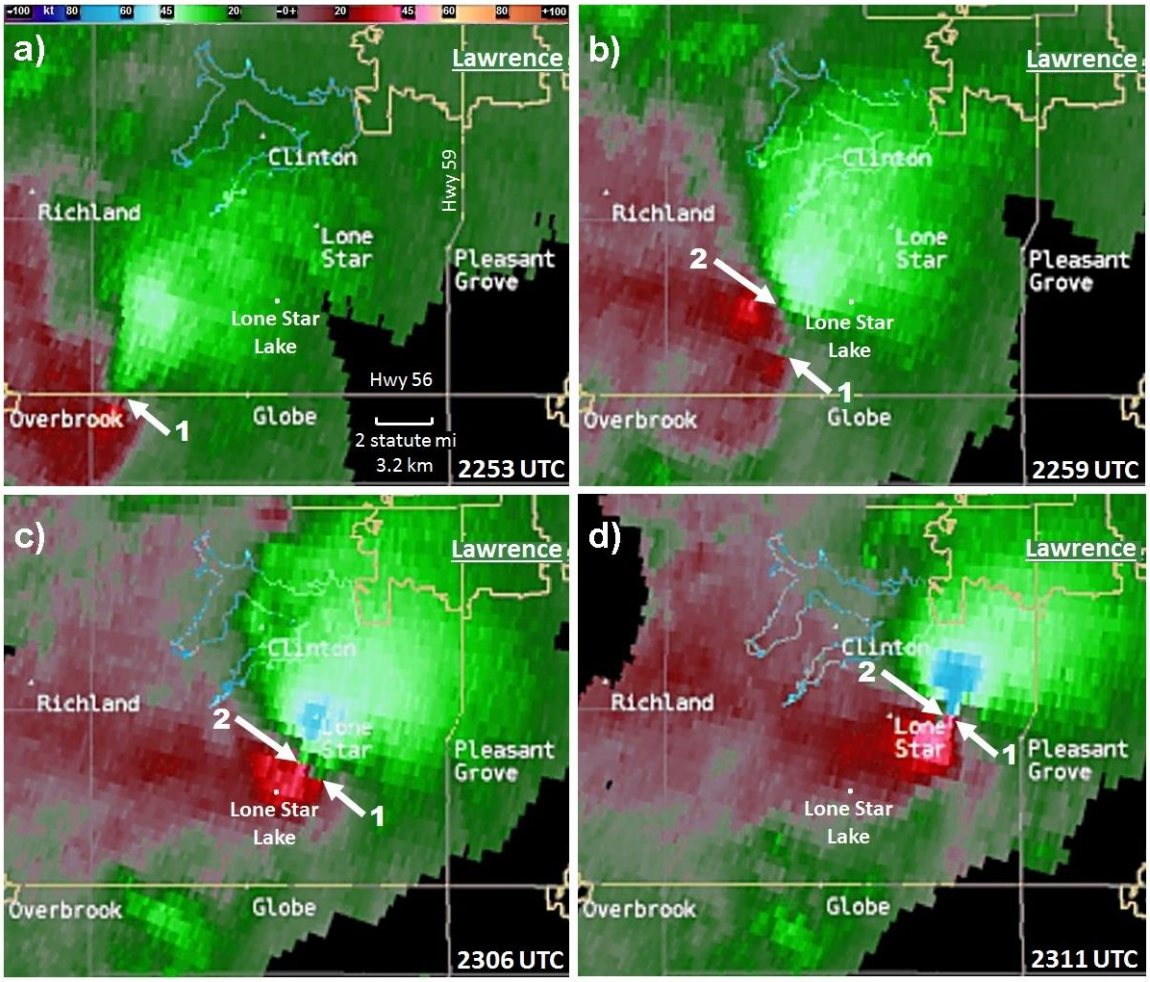

Figure 6. Storm-relative velocity (0.5 degree elevation) from Topeka NWS radar zoomed in on local area southwest of Lawrence, KS on 28 May 2019 at: a) 2253 UTC; b) 2259 UTC: c) 2306 UTC; and d) 2311 UTC. White arrow "1" indicates rotation associated with original mesocyclone; white arrow "2" indicates rotation associated with newer mesocyclone.

velocity couplets, but moving closer together as the northern mesocyclone intensified, appearing to interact with and accelerate the southern mesocyclone northeastward. Notice that, comparing Fig. 6c with Fig. 6b, the original mesocyclone was now less than a mile (1.6 km) to the southeast of the newer intensifying one, suggesting that the northern mesocyclone was influencing its motion. The ground survey in Fig. 1 also shows that both mesocyclones were producing tornadoes at this time, with the newer mesocyclone generating its own tornado beginning at the northeast corner of Lone Star Lake around 2305 UTC. Five minutes later by 2311 UTC (Fig. 6d), both mesocyclones and tornadoes had combined together into one large mesocyclone from which the large Lawrence-Linwood tornado was in progress near the start of its 29-mile (47 km) path.

Base reflectivity from the Topeka radar corresponding to the same times in Fig. 6 is shown in Fig. 7, with the location of mesocyclones from Fig, 6 plotted on the images. In Fig. 7b, a comma head of heavier precipitation (dark red), not seen around the original mesocyclone in Fig. 7a, was organizing around the new northern mesocyclone, suggesting (along with the intensification and inflow changes seen in Figs. 6b and 6c) that this newer circulation was evolving into the primary mesocyclone. The two mesocyclones continued to move closer together (Fig. 7c), with the northern one likely influencing the motion of the southern one. After the two circulations interacted and consolidated, the single large mesocyclone (Fig. 7d) produced a strong and widening tornado located near the center of the precipitation comma head of dark red base reflectivity.

4. Visual evolution

Figure 8a-b-c-d is a schematic summarizing the evolution of mesocyclones and tornadoes

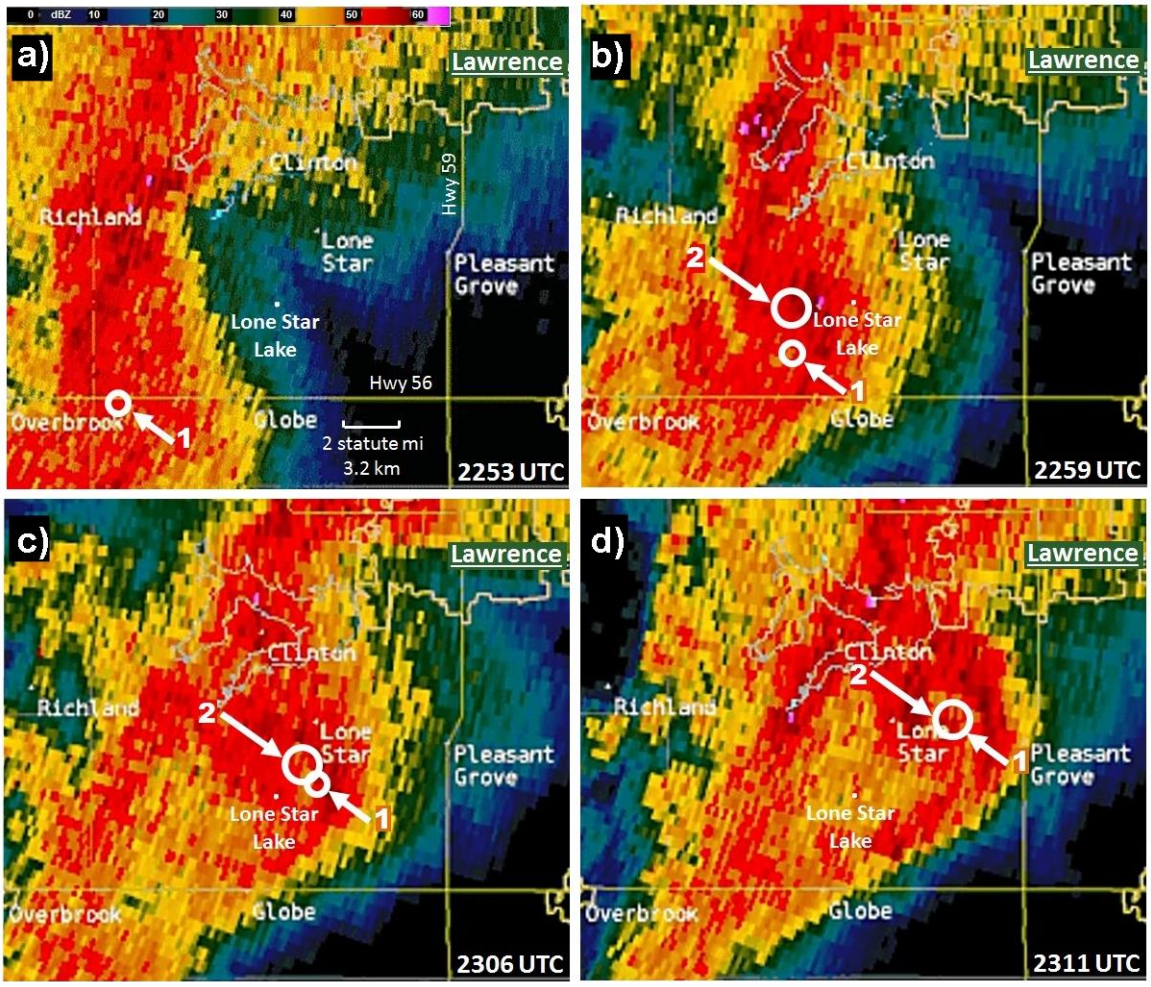

Figure 7. As in Fig. 6, except base reflectivity (0.5 degree elevation). White circles show locations of mesocyclones from rotation areas indicated in Fig. 6.

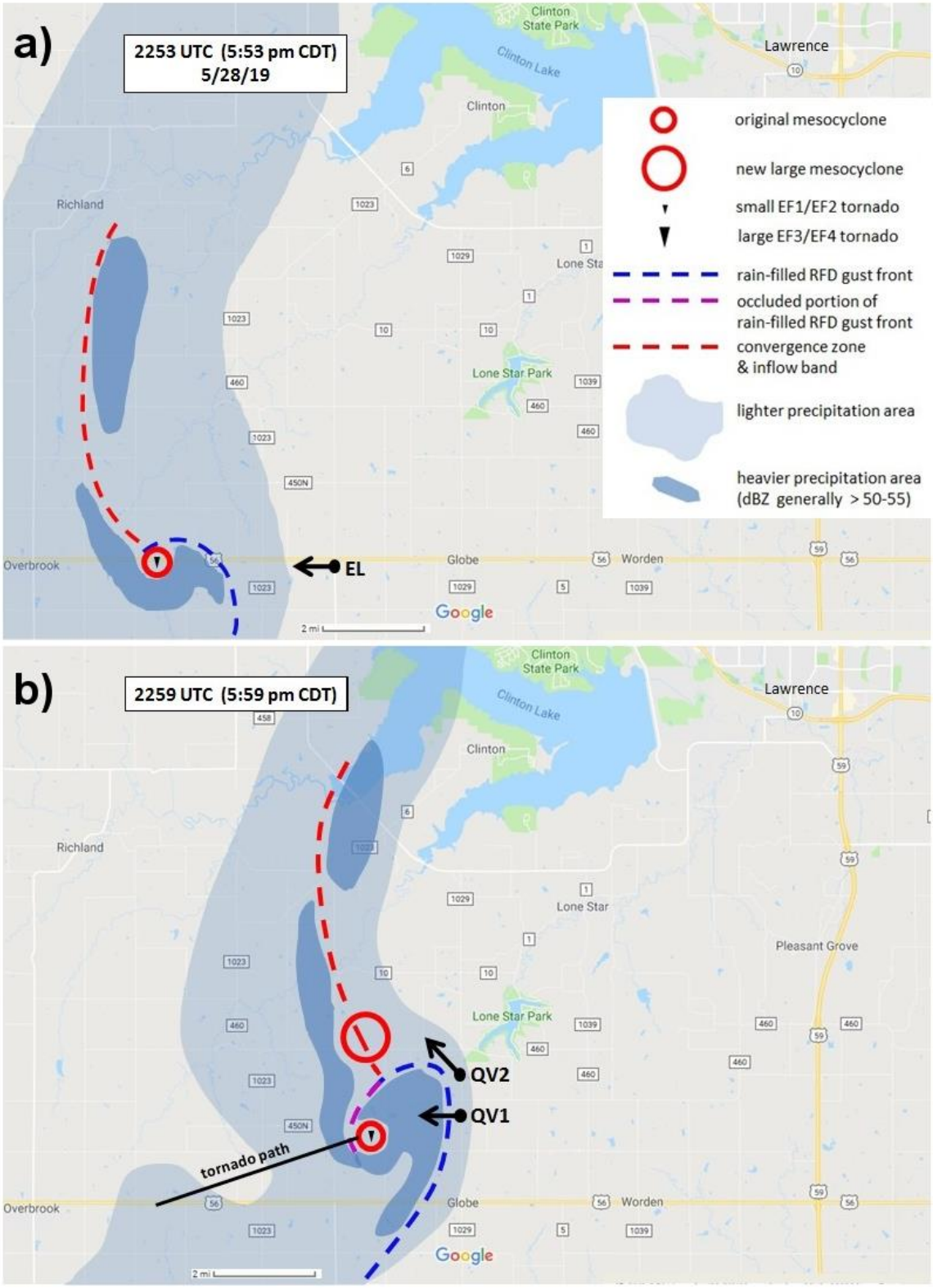

Figure 8a and 8b. Schematic showing evolution of mesocyclones and tornadoes southwest of Lawrence, KS on 28 May 2019, corresponding to same times as in Fig. 6a and 6b, and Fig. 7a and 7b. Key to relevant storm features is shown in a). Progressive tornado tracks, and video/photo locations referenced in text and in Figs. 9-14, are shown in black.

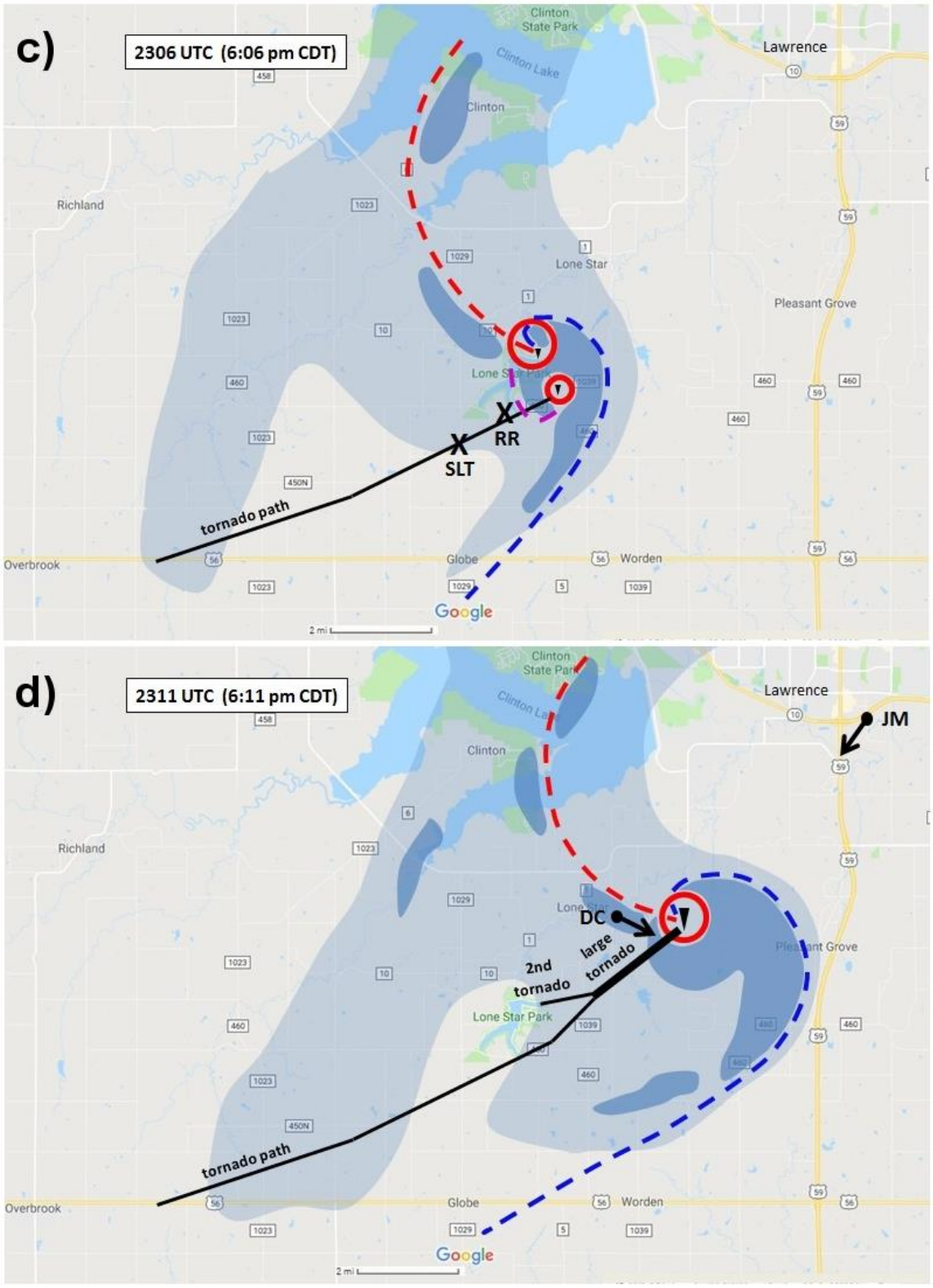

Figure 8c and 8d. As in Fig. 8a and 8b, except corresponding to same times as in Fig. 6c and 6d, and Fig. 7c and 7d. Key to relevant storm features is shown back in Fig. 8a.

Figure 9. Photo by Eric Lawson at 2151 UTC, looking west from location "EL" in Fig. 8a.

with the HP supercell, corresponding to the radar image times in Figs. 6 and 7. A key for annotated features is shown in Fig. 8a. Heavier precipitation areas near ground elevation are shown in darker blue-gray shading, *estimated* from combining visual observations by storm chasers with radar, the beam of which (even at lowest elevation angle) would cut through the storm some distance aloft due to earth curvature.

At 2253 UTC in Fig. 8a, the original mesocyclone and tornado were about to cross Highway 56. A couple minutes before this, Eric Lawson photographed the storm (Fig. 9) looking west from location "EL" in Fig. 8a. This image does not show much visual structure to the supercell, except that south of a low dark cloud base, part of the storm with radar rotation was wrapped in rain, confirmed by other storm chasers (Stormtrack forum 2019) who were driving on Highway 56 near the radar-indicated mesocyclone.

Comparing Figs. 8a and 8b, the original mesocyclone and tornado at 2259 UTC were becoming increasingly occluded (Doswell and Lemon 1979; Burgess et al. 1982) within an area of heavier precipitation as the gust front of the HP supercell's rain-filled RFD surged northeast. Two images from video looking west in Figs. 10a and 10b at roughly 2257 and 2258 UTC by Quincy Vagell (location "QV1" in Fig. 8b) show how quickly this RFD gust front and rain-filled area were evolving and surging northeastward. At this time, the continuing tornado from the occluded mesocyclone was well-hidden from view due to its rain-wrapped location one to one and a half miles (1.6 to 2.4 km) back behind the gust front or leading edge of the rain-filled RFD.

At the same time to the north in Fig. 8b, the large new mesocyclone discussed in the prior section was developing near where a convergence zone and inflow band into the supercell from the northwest met the RFD gust front. This developing mesocyclone was visible looking northwest in Fig. 11 (video image by Quincy Vagell at roughly 2259, location "QV2" in Fig. 8b), to the north of the surging rain-filled RFD seen in Fig. 10. This development and evolution is similar to the mesocyclone evolution model from Burgess et al. (1982), except that the new visible mesocyclone was forming to the north of the occluded one, instead of to the east or northeast.

By 2306 UTC in Fig. 8c, the deeply occluded mesocyclone and accompanying rain-wrapped tornado had already struck two vans of a storm tour company ("X" location marked "SLT" in Fig. 8c) while they were driving south toward Highway 56 to avoid the mesocyclone visible in Fig. 11, also seen in radar velocities from Fig. 6b in the prior section. This same rain-wrapped tornado nearly struck storm chaser Robert Reynolds ("X" location marked "RR" in Fig. 8c)

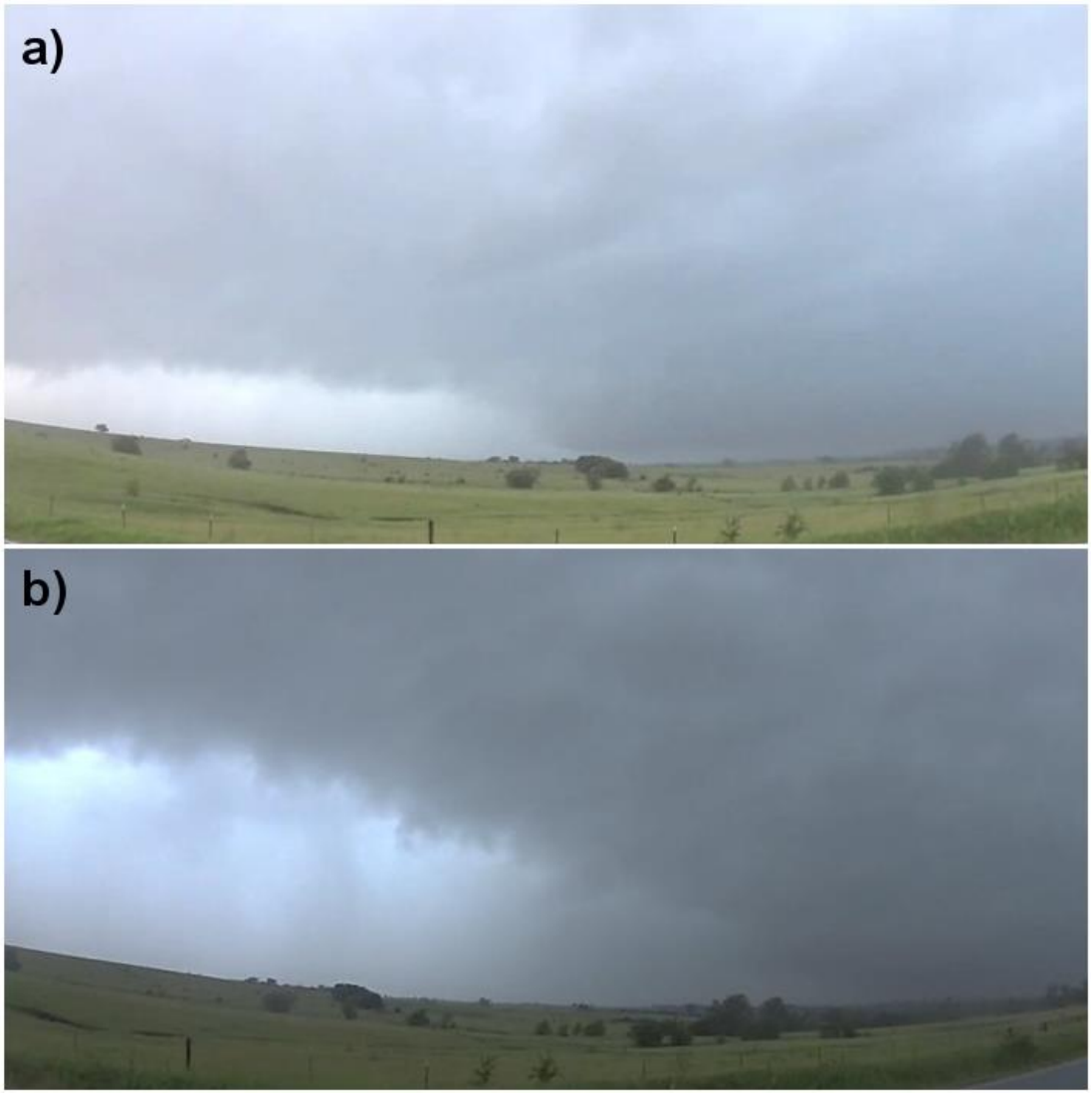

Figure 10. Images from video by Quincy Vagell, looking west at rain-filled RFD gust front from location "QV1" in Fig. 8b at approximately: a) 2257 UTC; and b) 2258 UTC.

Figure 11. Image from video by Quincy Vagell, looking northwest from location "QV2" in Fig. 8b at approximately 2259 UTC.

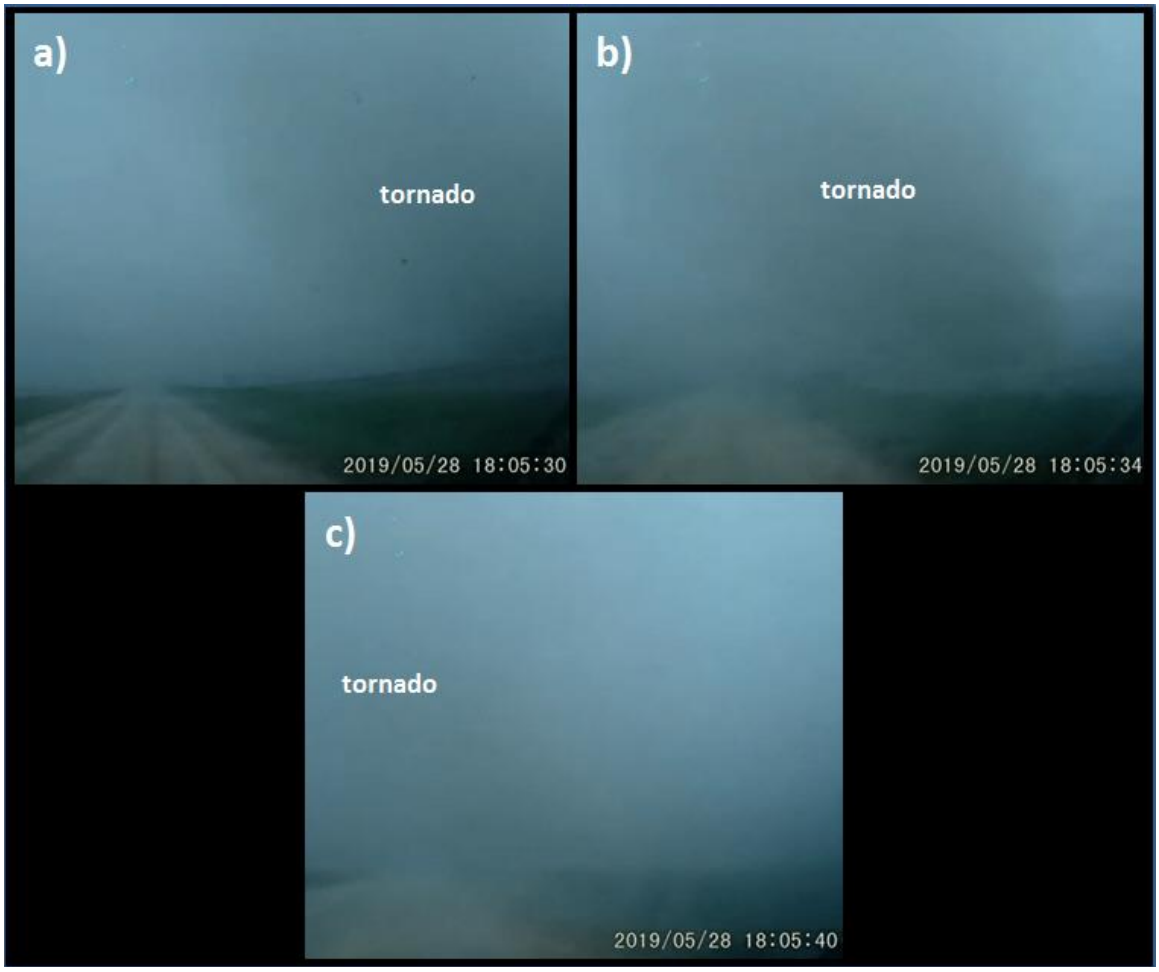

Figure 12. Successive video images (a-b-c) of tornado emerging briefly from rain, approximately 5 seconds apart, by Robert Reynolds, looking east from location "RR" in Fig. 8c at 2305 UTC.

Figure 13. Image from video of newly formed large tornado (left center) by Dalton Coody, looking southeast from location "DC" in Fig. 8d at approximately 2310 UTC.

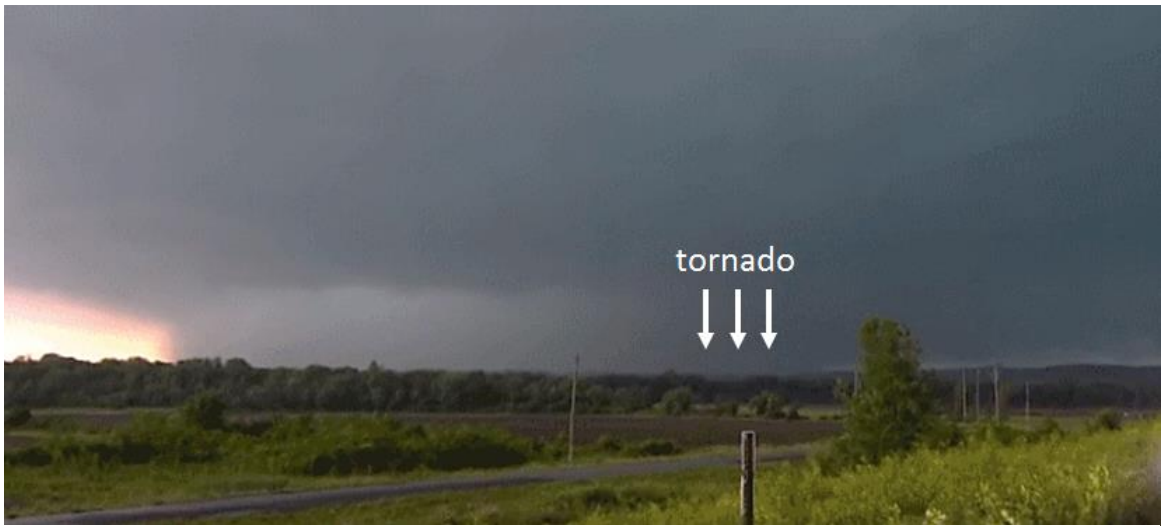

Figure 14. Image from video by Jack Miller, looking southwest from Lawrence, KS (location "JM" in Fig. 8d) at approximately 2312 UTC.

two to three minutes later on the south side of Lone Star Lake. Images from Reynolds' video looking east in Fig. 12a-b-c show the tornado as it became visible briefly in the rain and crossed the road in front of him.

Notice too in Fig. 8c how the developing northern mesocyclone had become well-established and, through its intensification and size, was apparently interacting with and influencing the movement of the occluded southern one, accelerating it and moving it closer (refer back to the radar imagery in section 3). Although no photography is available showing the northern mesocyclone at this point, it had begun producing a new tornado (confirmed by tree damage) at the northeast end of Lone Star Lake, and may have now been at least partially wrapped in rain as the rain-filled RFD surge became incorporated into its circulation.

By 2311 UTC in Fig. 8d, both mesocyclones and their accompanying tornadoes had combined into one large circulation, with a large and widening tornado now in progress destroying trees in a wooded area a couple miles east-northeast of Lone Star Lake. This large tornado was visible briefly on video by Dalton Coody looking southeast (see Fig. 13 and location "DC" in Fig. 8d) shortly after the two mesocyclones consolidated into one. However, from video by Jack Miller (Fig. 14, location "JM" in Fig. 8d) looking southwest from the south side of Lawrence at nearly the same time, this tornado was not really visible, emphasizing the consistent "HP" nature of this supercell.

5. Comparison with Hesston-Goessel tornado interaction in 1990

Fujita (1992) and Davies et al. (1994) documented the interaction and consolidation of two long-track mesocyclones and tornadoes within a classic supercell (Doswell and Burgess 1993) on March 13, 1990 between Hesston and Goessel, KS. Figure 15 from Fujita (1992), shows this interaction. Comparing Fig. 15 with a close up of the author's ground survey in Fig. 16 of the two tornado tracks "merging" on May 28, 2019 suggests similarities in evolution.

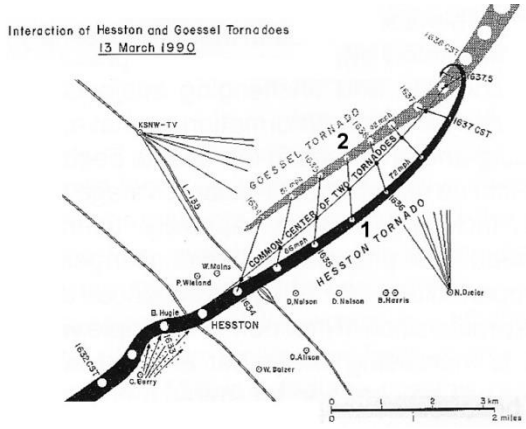

Figure 15. Graphic showing tornado tracks associated with the interaction of two mesocyclones between Hesston and Goessel, KS on March 13, 1990, from Fujita (1992). Labels "1" and "2" have been added to reference tornadoes seen in Fig. 17.

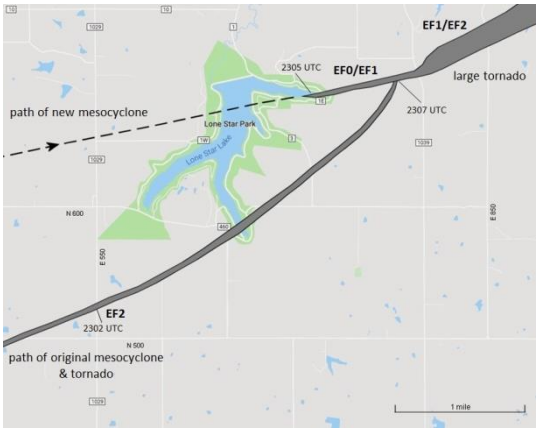

Figure 16. Close up view of tornado tracks between approximately 2300 UTC and 2310 UTC on 28 May 2019, from author's damage survey near Lone Star Lake, KS.

In both cases, a new mesocyclone and tornado developed to the north of an occluding mesocyclone and tornado that had been on the ground for a number of miles (see photo in Fig. 17, from March 13, 1990). The main difference between the two events is that the May 28 supercell was HP rather than classic in nature, so that the combining and consolidation of mesocyclone and tornado circulations was not visible to storm spotters and chasers due to the rain-wrapped structure of the storm.

To the author's knowledge, this is the first documentation of an interaction and consolidation of two long-track mesocyclones and tornadoes *within an HP supercell*. Such interactions probably happen occasionally, but are difficult to document due to the lack of visibility within and around HP supercell storms.

6. Implications for spotter training regarding HP supercells

The rapid evolution in the early tornadic stages of the Lawrence-Linwood HP supercell and the storm tour accident involving an unexpected rain-wrapped tornado have implications for future spotter training about HP supercell storms.

The author's discussion with the tour company operator (R. Hill, personal communication, 2019) regarding decisions and positioning prior to the encounter with the tornado reveals that the tour was reacting to the northern mesocyclone that was visually evident (e.g., Fig. 11 in section 4) with a broad velocity couplet on radar (e.g., Fig. 6b in section 3). The tour company was heading south to avoid this northern mesocyclone that was moving east-northeast across their path, and did not understand that a rain-wrapped tornado was occluded deep within the rain-filled RFD they were driving into, away from the newly developing mesocyclone.

At the time of the incident, no confirmations or reports of tornadoes had appeared via local storm reports or within the text of NWS warnings. One way to deduce that an occluded

Figure 17. Photo by Nancy Franzen on March 13, 1990 showing mesocyclones and tornadoes (see labels "1" and "2" in Fig. 15) interacting between Hesston and Goessel, KS. View is looking southwest from 5 miles northeast of Hesston.

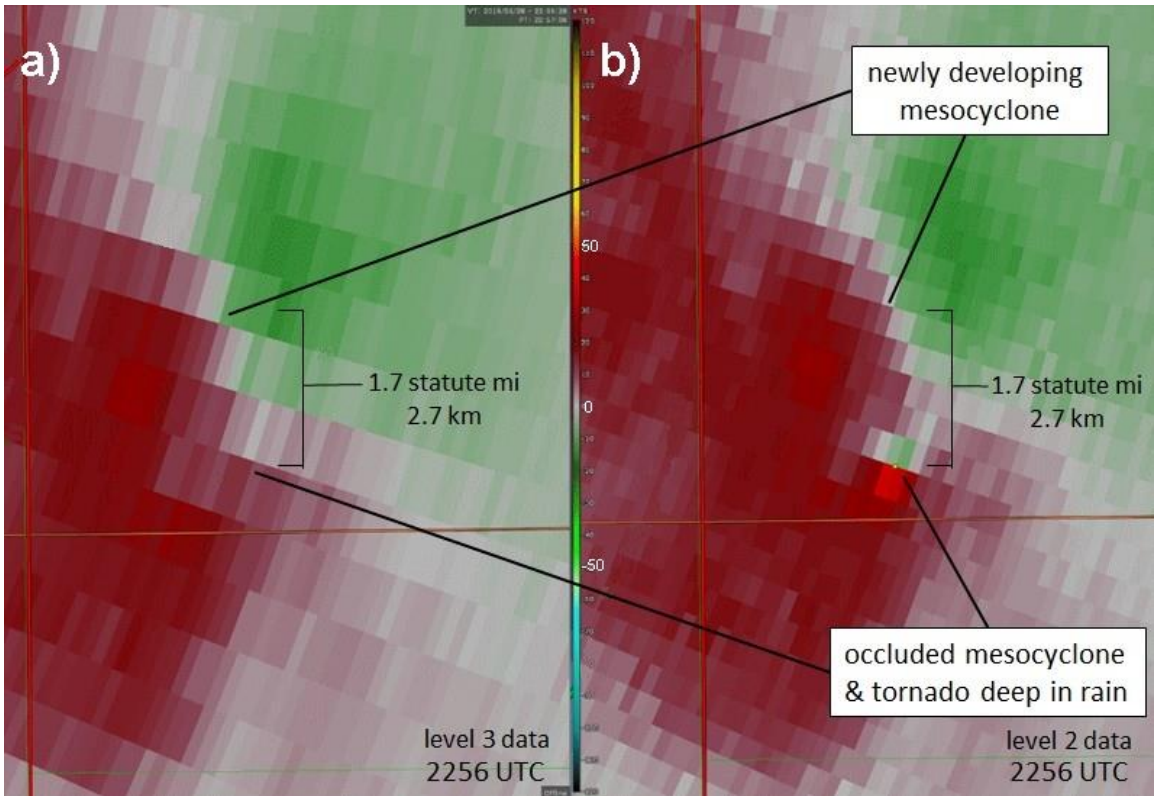

Figure 18. Storm-relative velocity (0.5 degree elevation) from Topeka NWS radar zoomed in on local area just southwest of Lone Star Lake, KS on 28 May 2019 at 2256 UTC: a) is level 3 radar data displayed using *GRLevel3* software; and b) is level 2 radar data displayed using *GRLevel2 Analyst.*

tornado could be occurring far back in the rain-filled RFD would be careful attention to velocity couplets on radar, indicating the presence of a mesocyclone. This brings up a significant issue regarding quality of radar data used in mobile settings.

Figure 18 shows storm-relative velocity fields from the Topeka radar via level 3 data (Fig. 18a) compared to higher resolution level 2 data (Fig. 18b) at 2256 UTC, zoomed in on the area southwest of Lawrence near Lone Star Lake and roughly six minutes before the storm tour accident. Notice how the small velocity couplet associated with the rain-wrapped occluded mesocyclone and tornado was discernible in Fig. 18b with the higher resolution level 2 data, but was difficult to find in the lower resolution level 3 data (Fig. 18a). It is important to note that the tour company was using a real-time radar application based on level 3 data, and not level 2. Many spotters and storm chasers may not understand the impact of differing resolutions between these levels of data, which can be crucial in a situation where mesocyclones (and possible tornadoes) are not visible due to rain-wrapping of heavier precipitation as on May 28. This difference should be made clear in training for spotters (and storm chasers) who use mobile radar applications.

From a visual standpoint, spotters and chasers also need to be increasingly aware of how deeply occluded a rain-wrapped tornado can be within the rain-filled RFD of a HP supercell. Because many HP supercells have mesocyclones that occur near the front flank of the storm (Moller et al. 1994), there may be a tendency for spotters and chasers to discount tornado potential some distance away from the front flank within a surging rain-filled RFD. But as this case shows, tornadoes can be located deep within the occluded "inside" portion of the surging gust front where it curls far back into the rain (see Fig. 8b in section 4, and inset radar image in Fig. 19). Again, it is notable that the occluded tornado that struck the tour company was as much as a mile and a half (1.6 to 2.4 km) behind the leading edge gust front of the surging rain-filled RFD.

Figure 19 also shows a panoramic view constructed from video by the storm tour company from a location approximately 3 miles (4.8 km) north of Globe, KS at roughly 2300

Figure 19. Panoramic view from video by Silver Lining Tours, looking south through west (from location "SLT" in inset) at approximately 2300 UTC, with relevant features labeled. Insert is base reflectivity as in Fig. 7b, but zoomed in on local area near Lone Star Lake, KS, with relevant features indicated as described in key to Fig. 8a.

UTC (see location "SLT" marked on the radar inset in Fig. 19). The view is looking south through west at the approaching and surging rain-filled RFD gust front, with the newly developing mesocyclone also visible to the west. The occluded tornado, not visible or confirmed via media at this point, was located deep within the right "inside" portion of the rain-filled area (see arrow on photo in Fig. 19) comprising the surging RFD when looking southwest. In earlier images, when viewed toward the west from a position father south looking across the rain-filled RFD (see Fig. 10 from section 4), the tornado was located left of center, also well back in the rain when viewed from the east.

Unfortunately, much spotter training is by necessity focused on classic supercells where features are more visible for teaching purposes. In such training, positioning is based on visual location of the mesocyclone area via a lowering or wall cloud (Moller et al. 1994) with the goal to stay south or southeast of that feature, away from its path of motion. But with HP supercells, such features are usually hidden by rain and not visible due to rain-filled RFD gust fronts that wrap into the mesocyclone.. In a rapidly evolving situation with a northeastward-moving HP supercell and a developing mesocyclone north of a rain-filled RFD as on May 28, there may be a tendency for spotters and chasers to focus on the visible mesocyclone and move south into a surging rain-filled area to stay clear of the more "visually compelling" area of threat. On HP supercells, spotters and chasers should train themselves to recognize rain-filled RFDs and their leading edge gust fronts, and to anticipate possible surges or rapid evolutions to stay out of the way of such features..

Recognizing and understanding the potential dangers of RFD areas, such as strong winds (e.g., Markowski 2001; Wakimoto et al. 2016) *and occluded tornadoes* (e.g., this study) with HP supercells should be a key part of spotter training materials, particularly in rapidly evolving settings where there are multiple spotting features to assess. From a spotting perspective, HP supercells with their lack of visual clarity (Moller et al. 1994) are often more visibly complex than classic supercells, yet are the most common type of supercell (Doswell and Burgess 1993). Such storms should be given a wide berth by both spotters and chasers, allowing plenty of room for adjusting position when these storms evolve rapidly. Careful and consistent radar monitoring for velocity couplets within rain-filled areas using mobile radar applications based on *level 2 data* should be emphasized, along with recognizing visual clues such as rain-filled RFD gust fronts that may contain occluded mesocyclones and rain-wrapped tornadoes well back from the leading edge of the gust front.

7. Conclusion

This study has documented the evolution of the early tornadic phase of the 28 May 2019 HP supercell in northeast Kansas, including an interaction and consolidation of long-track

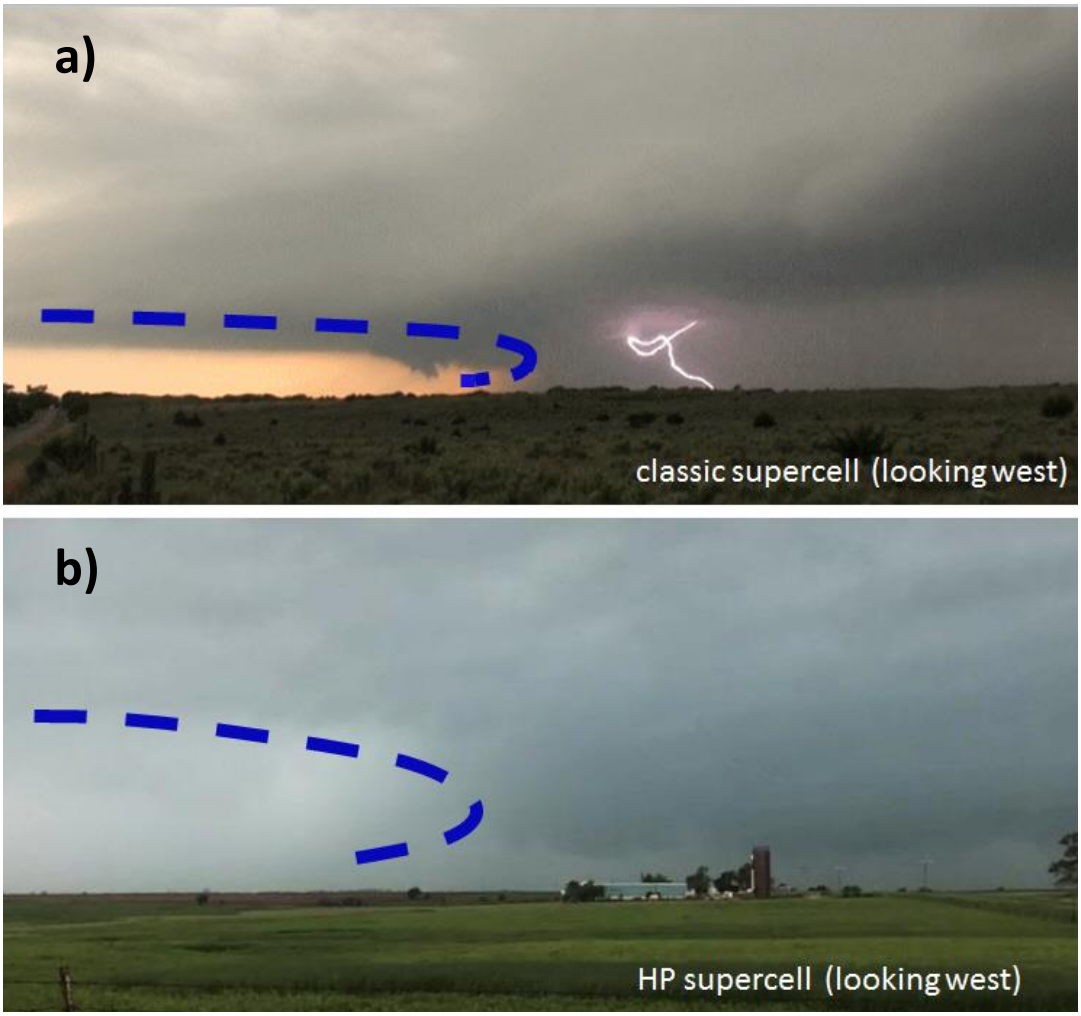

Figure 20. Images of a) classic supercell, from video by the author, and b) HP supercell, photo by Eric Lawson (same image as Fig. 2), looking west from similar angles. This is an example of how the RFD gust front (thick blue dashed line) appears quite different between the two supercell types.

Figure 21. Photo of HP supercell in north-central Kansas (15 June 1992) looking west, by the author.

mesocyclones and tornadoes similar to the Hesston-Goessel event in 1990 (Fujita 1992; Davies 1994). Though such interactions undoubtedly occur on occasion, this may be the first time such an evolution has been documented within a HP supercell where it would not normally be visible. Both mesocyclones and their interplay presented a confusing spotter scenario that contributed to a storm tour incident that occurred near Lone Star Lake, southwest of Lawrence, KS. As a result, a primary motivation for this paper is to suggest stronger emphasis on HP supercells in training for spotters (and storm chasers), even for those who are relatively experienced.

The prior section discussed important spotter issues with HP supercells, such as tornadoes buried deep within rain-filled RFDs, multiple mesocyclone features (some visible, some not), and differences in resolution between mobile radar applications (level 2 vs. level 3 data) that can affect recognition of mesocyclones via velocity products. Future spotter training material from NWS and other sources should more specifically address HP supercell issues, correlating radar and photo/video images (e.g., Fig. 19 from the prior section) along with schematics to increase understanding of common features that are conceptually the same, but that appear quite different visually between HP and classic supercells (e.g., see Fig. 20).

With some HP supercells, particularly in the central or high Plains of the United States where visibility near supercell storms is often better (Moller et al. 1994), the portion of a HP supercell to avoid may be visually evident. An example is Fig. 21, where the dark area of heavy precipitation behind the RFD gust front and within the rain-filled RFD was apparent and even quite threatening in appearance.

However, comparing Fig. 20b to Fig. 21, the RFD gust front and rain-filled RFD were more difficult to discern on May 28, and were less compelling visually than in Fig. 21. Such differences should be discussed and accentuated in training materials to help prepare spotters and chasers for difficult visual identification issues of features on many HP supercells.

Finally, the inclination for spotters and chasers to move southward into a rain-filled RFD area to avoid threatening visual characteristics that suggest new mesocyclone development near the front flank of a HP supercell (as on May 28) should be acknowledged and corrected in future spotter training materials. Spotters and chasers can learn through repeated education to more readily discern rain-filled RFD areas that may contain dangerous winds and even deeply occluded tornadoes, as on May 28. Understanding and anticipating the potential for RFD surges and rapid evolution in some HP supercells will result in safer and more effective spotter positioning, allowing space and time for error when fast developments do occur. Training improvements concerning HP supercells can go a significant way toward avoiding unfortunate spotter and chaser incidents in the future.

ACKNOWLEDGMENTS

Eric Lawson, Quincy Vagell, Robert Reynolds, Dalton Coody, Jack Miller, and Roger Hill are gratefully acknowledged for sharing their video and photography for this study.

REFERENCES

Burgess, D. W., V. T. Wood, and R. A. Brown, 1982: Mesocyclone evolution statistics. Preprints, *12th Conf. on Severe Local Storms*, San Antonio, TX, Amer. Meteor. Soc., 422–424.

Davies, J. M., C. A. Doswell III, D. W. Burgess, and J. F. Weaver, 1994: Some noteworthy aspects of the Hesston, Kansas, tornado family of 13 March 1990. *Bull. Amer. Meteor. Soc.*, **75**, 1007–1017.

Doswell, C. A. III, and D. W. Burgess, 1993: Conceptual models of tornadoes and tornadic storms. *The Tornado: Its Structure, Dynamics, Prediction, and Hazards*, Geophys. Monogr., No. 79, Amer. Geophys. Union, 161–172.

Fujita, T. T., 1992: Memoirs of an Effort to Unlock the Mystery of Severe Storms During the 50 Years, 1942-1992. University of Chicago, 298 pp.

Johns, R. H., J. M. Davies, and P. W. Leftwich, 1993: Some wind and instability parameters associated with strong and violent tornadoes. 2. Variations in the combinations of wind and instability parameters. *The Tornado: Its Structure, Dynamics, Prediction, and Hazards*, Geophys. Monogr., No. 79, Amer. Geophys. Union, 583–590.

Lemon, L. R., and C. A. Doswell III, 1979: Severe thunderstorm evolution and mesocyclone structure as related to tornadogenesis. *Mon. Wea. Rev*., **107**, 1184–1197.

Markowski, P. M., 2001: Hook echoes and rear-flank downdrafts: A review. *Mon. Wea. Rev*., **130**, 852–876.

Moller, A. R., C. A. Doswell III, M. P. Foster, and G. R. Woodall, 1994: The operational recognition of supercell thunderstorm environments and storm structures. *Wea. Forecasting*, **9**, 327–347.

Palmén, E., and C. W. Newton, 1969: *Atmospheric circulation systems.* Academic Press, 603 pp.

Stormtrack forum, 2019: Silver Lining Tours vans rolled in Kansas. Accessed 15 September 2019, https://stormtrack.org/community/threads/silver-lining-tours-vans-rolled-in-kansas.30901/.

Thompson, R. L., R. Edwards, and C. M. Mead, 2004: An update to the supercell composite and significant tornado parameters. *22nd Conf. Severe Local Storms*, Hyannis MA, Amer. Meteor. Soc., P8.1.

Wakimoto, R. M., N. T. Atkins, K. M. Butler, H. B. Bluestein, K. Thiem, J. C. Snyder, J. Houser, K. Kosiba, and J. Wurman, 2016: Aerial damage survey of the 2013 El Reno tornado combined with mobile radar data. *Mon. Wea. Rev*., **144**, 1749–1776.